Phase-Approaching Stimulation Sequence for SSVEP-Based BCI: A Practical Use in VR/AR HMD

Hao-Teng Hsu, Kuo-Kai Shyu, *Senior Member, IEEE*, Chuan-Chih Hsu, Lung-Hao Lee, *Member, IEEE*, and Po-Lei Lee, *Member, IEEE*

***Abstract*— Steady-state visual evoked potential (SSVEP) has been used to implement brain-computer interface (BCI) due to its advantages of high information transfer rate (ITR) and high accuracy. In recent years, owing to the developments of head-mounted device (HMD), the HMD has become a popular device to implement SSVEP–based BCI. However, an HMD with fixed frame rate only can flash at its subharmonic frequencies which limits the available number of stimulation frequencies for SSVEP-based BCI. In order to increase the number of available commands for SSVEP-based BCI, we proposed a phase-approaching (PA) method to generate visual stimulation sequences at user-specified frequency on an HMD. The flickering sequence generated by our PA method (PAS sequence) tries to approximate user-specified stimulation frequency by means of minimizing the difference of accumulated phases between our PAS sequence and the ideal wave of user-specified frequency. The generated sequence of PA method determines the brightness state for each frame to approach the accumulated phase of the ideal wave. The SSVEPs evoked from stimulators, driven by PAS sequences, were analyzed using canonical correlation analysis (CCA) to identify user's gazed target. In this study, a six-command SSVEP-based BCI was designed to operate a flying drone. The ITR and detection accuracy are 36.84 bits/min and 93.30%, respectively.**

***Index Terms*— Phase-approaching method, steady state visual evoked potential, canonical correlation accuracy, brain computer interface.**

I. Introduction

BRAIN computer interface (BCI) is a promising technique which translates user's intention through the brain-wave recordings into communication signals. Several research groups utilized electroencephalogram (EEG) signals, such as slow cortical potential (SCP) [1], readiness potential [2], P300 [3], event-related desynchronization/synchronization (ERD/ERS) [4], flash visual evoked potential (FVEP) [5], and steady-state visual evoked potential (SSVEP) [6], as control signals to implement BCI systems. The SSVEP has been widely applied to realize various BCI applications, due to its high information transfer rate (ITR) and easy for implementation [6]–[9]. It is known that an SSVEP-based BCI system contains a visual stimulator, an EEG acquisition equipment, and a personal computer (PC) for signal processing. However, the bulky size of CRT/LCD could hamper the mobility of the BCI system. Therefore, a head-mounted device (HMD), which has the advantages of easy-to-wear and high portability, was chosen for visual stimulation in our SSVEP-based BCI system.

In recent years, some research groups had utilized HMDs (e.g., Oculus Rift, HTC VIVE, Microsoft HoloLens, etc.), to implement BCI systems. Koo *et al.* proposed the SSVEP-based BCI with Oculus Rift [10]. They reported that the virtual reality (VR) HMD improved users' engagements in operating the BCI system because users paid more attention in the immersive environment compared with the LCD monitor in open space. Wang *et al.* utilized HTC VIVE to implement a wearable SSVEP-based BCI [11]. They used gyroscope to eliminate the influence of head movement which led to better accuracy by removing motion artifacts. Si-Mohammed *et al.* demonstrated the feasibility of using augmented reality (AR) HMD to implement SSVEP-based BCI system [12]. They reported that the AR HMD had successfully used to induce subjects' SSVEPs and had achieved high detection accuracies. They suggested the placements of the virtual objects for visual stimulations should be designed as fixed objects and merged with the real environment. In our study, we intended to use SSVEP induced from HMD to control a flying drone. The AR HMD, which allows subjects to see and sense their peripheral environments, was chosen to induce subjects' SSVEP and controlled a flying drone. The virtual objects in HoloLens were designed as flickering objects with distinct designated frequencies and subjects' SSVEPs induced by different stimulation frequencies were used to control corresponding operation commands of the flying drone. The high portability of HoloLens could be helpful to promote the applications of SSVEP-based BCI.

Manuscript received May 22, 2021; revised September 30, 2021; accepted November 15, 2021. Date of publication November 30, 2021; date of current version January 11, 2022. This work was supported by the National Central University, Ministry of Science and Technology (MOST) through Pervasive Artificial Intelligence Research (PAIR) Labs under Grant 110-2634-F-008-007- and Grant 109-2221-E-008-074-. *(Corresponding author: Po-Lei Lee.)*

This work involved human subjects in its research. Approval of all ethical and experimental procedures and protocols was granted by the Ethics Committee of Institutional Review Board, Tao-Yuan General Hospital, Taiwan.

Hao-Teng Hsu, Kuo-Kai Shyu, Lung-Hao Lee, and Po-Lei Lee are with the Department of Electrical Engineering, National Central University, Taoyuan City 32001, Taiwan (e-mail: fifaworld91@g.ncu.edu.tw; kkshyu@ee.ncu.edu.tw; lhlee@ee.ncu.edu.tw; pllee@ee.ncu.edu.tw).

Chuan-Chih Hsu is with the Division of Cardiovascular Surgery, Taipei Medical University Hospital, Taipei 110, Taiwan (e-mail: cchsu1967@hotmail.com).

Digital Object Identifier 10.1109/TNSRE.2021.3131779

Nevertheless, the available flickering frequencies for inducing SSVEP using AR HMD are limited. It faces the same problem as all the current display devices, including CRT, LCD VR and AR HMDs. Owing to the fixed refreshing rate (e.g., 60 Hz), the virtual objects only can be flickered at frequencies achieved by repetitive flashing segments, in which each flashing segment contains a fixed number of frames, illuminated at bright or dark states. For example, a screen with 60Hz frame rate can achieve the 12Hz flickering frequency with five frames, either the combination of two white plus three dark frames or three white plus two dark frames. Therefore, for a preset refreshing frequency, the flickering frequencies for the virtual objects only can be chosen at the few subharmonic frequencies of the refreshing rate. For a displayer at 60 Hz refreshing rate, the available stimulation frequencies are $60/n$ (n is an integer number) which results in available stimulation frequencies at 30, 20, 15, 12, 10, 8.57, 7.5, 6.67 and 6 Hz for $n = 2, 3, 4, 5, 6, 7, 8, 9,$ and 10, respectively. Volosyak *et al*. even indicated that only five subharmonic frequencies (6.67, 7.50, 8.57, 10, and 12 Hz) of a 60 Hz display system, were suitable for designing BCI commands [13]. Due to the development of display technologies, some studies have adopted display devices with higher refreshing rate, such as 72 Hz [14], 90 Hz [15], and 120 Hz [16], to increase the available number of BCI commands. However, since the majority of popular consumer products (standalone HMD) is based on 60 Hz refreshing rate, a frequency approximation method, which enables the synthesis of user-specified stimulation frequency on a 60 Hz display device, is worthy to be developed.

At least two frequency approximation approaches have been proposed in previous literatures, one is the sampled sinusoidal stimulation method [17] and the other is the mixing frequency method [18]. For the sampled sinusoidal stimulation method, Chen *et al.* (2014) utilized a 60 Hz display device to achieve user-specified stimulation frequencies lower than 16Hz. The luminance was adjusted in accordance with the reference signal of a sinusoidal wave to synthesize the intended stimulation frequency. The synthesized stimulation frequencies were designed about one-fourth lower than the frequency of the screen refreshing rate, according to sampling theorem. Regarding the mixing- frequency method, Nakanishi *et al.* (2014) constructed user-specified frequency by mixing the stimulation sequences from two neighboring sub-harmonic frequencies. For some stimulation frequencies, the user-specified frequency is away from the two neighboring sub-harmonic frequencies, so that the stimulation states might change frequently between the two sub-harmonic frequencies and result in larger phase variation.

In this study, we proposed a phase-approaching (PA) method to approximate user-specified stimulation frequency by means of minimizing the difference of accumulated phases between the sequences of our PA method and the ideal stimulation wave. The generated sequence of PA method determines the brightness state for each frame to approach the accumulated phase of the ideal wave. The present work has been used to implement a six-command wearable SSVEP-based BCI at high stimulation frequencies, close to half of the screen refreshing rate. The PA method can increase the available number of BCI commands on an HMD.

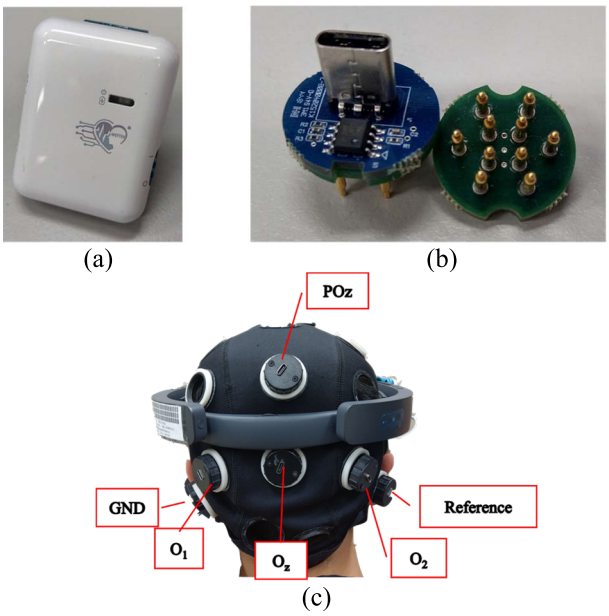

Fig. 1. (a) Four-channel EEG recorder. (b) Dry electrodes. (c) The deployment of EEG electrodes for SSVEP measurement.

II. Materials and Methods

A. Subjects and EEG Recordings

Twenty volunteers, including seventeen males and three females (22.35 ± 3.38 years old) who had no history of clinical visual disease with corrected Snellen visual acuity of 6/6 or better were recruited in this study. In this study, the EEG signals were recorded using a four-channel dry-electrode EEG recorder (InMex EEG, WellFulfill Co., Taiwan) (as shown in Fig. 1(a)), including an integrated analog front-end chip ADS1299 (Texas Instruments Co.), an ultralow-power microcontroller MSP430F5438a (Texas Instrument, United States), and a Bluetooth module for wireless data transmission. Each EEG dry electrode is constructed by 10 spring-loaded copper pins and the size of the dry electrode was designed in disk shape with 1cm diameter (as shown in Fig. 1(b)). The dry EEG electrodes were placed on O_z, O_1, O_2, and PO_z positions according to international 10-20 system [19] (as shown in Fig. 1(c)). The EEG signals were recorded at 1 kHz with 24-bits resolution and pre-filtered within 0.5-50 Hz (3th-order Butterworth IIR filter) for the following real-time BCI signal processing.

B. Experiment Tasks and Visual Stimuli

Fig. 2 shows the system architecture of our proposed wearable SSVEP-based BCI system. Subjects were requested to participate in an investigation study and an application study, approved by the Ethics Committee of Institutional Review Board (IRB), Tao-Yuan General Hospital, Taiwan (TYGH107055). The investigation study was designed to validate the frequency of induced SSVEP was the same as

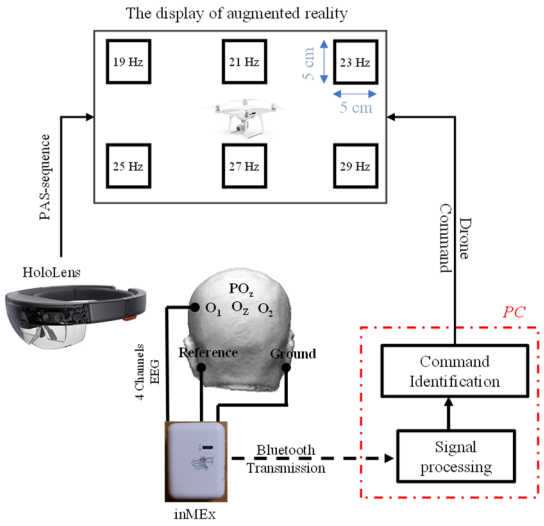

Fig. 2. The system architecture of our proposed wearable SSVEP-based BCI system.

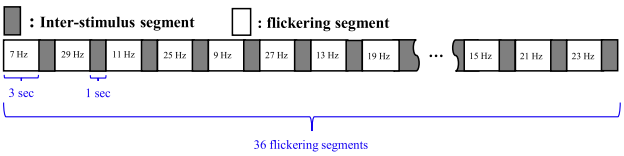

Fig. 3. The experiment protocol in the investigation study.

the flickering frequency of the virtual object. The application study was designed to study the capability of our proposed BCI system to control a flying drone (Phantom 4, DJI Co.).

In the investigation study, one virtual object, located at two-meter distance and upper left corner in front of our volunteer, was created with 5 cm × 5 cm size (1.43° subtended visual angle) in a 2D square shape (see Fig. 2). Subjects were requested to gaze the central virtual object for 144 s, including 36 flickering segments (see Fig. 3). The virtual object was driven by PA method (see below) to generate designed frequencies. Each flickering segment had 3s flickering period with another 1s blank screen to avoid inter-stimulus confusion of SSVEPs. According to [20], human SSVEP can be induced by gazing at flashing lights with flickering frequencies ranged from 6Hz to 100Hz. Therefore, only the stimulation frequencies above 6Hz (≥6 Hz) and below half of the screen refreshing frequency (≤30 Hz) were chosen in this study. The flickering frequency, f_{stim}, in each flickering segment was randomly chosen from twelve flickering frequencies, which were the odd frequencies below half of the screen refreshing frequency, i.e., 7, 9, . . . , 29Hz. Each stimulation frequency was guaranteed to appear three times in an investigation study.

For the application study, six virtual objects with distinct frequencies were allocated on subjects' visual fields. Each virtual object represented a function of a flying drone with an action indication on it. Subjects were requested to operate a drone by gazing at corresponding flying actions to complete a flight course. We considered the higher stimulation frequencies usually achieved more comfortable visualization

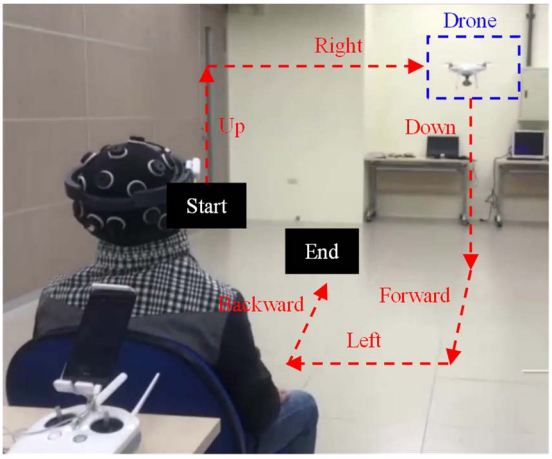

(a)

(b)

Fig. 4. (a) Subjects were instructed to complete a preset flight course "Up → Right → Down → Forward → Left → Backward" for two times, (b) the subject I who was wearing the HoloLens, the dry-electrode EEG cap and the four-channel inMEx system.

due to flickering fusion effect [21]. The six frequencies in the higher frequency portion among the twelve stimulation frequencies were chosen, which were 19, 21, 23, 25, 27, and 29 Hz, designated as f_1, $f_2, \ldots,$ and f_6, respectively, to control the six drone movement commands (f_1: Backward; f_2: Up; f_3: Forward; f_4: Left; f_5: Down, f_6: Right). The six stimulation frequencies were designated to the six virtual objects in 2 × 3 array placement, located at two-meter visual distance in front of our subjects (see Fig. 2). Subjects were instructed to complete a preset flight course "Up → Right → Down → Forward → Left → Backward" for two times (see Fig. 4(a)). For the occurrence of wrong execution commands, the drone could fly deviating from the aforementioned flight course. We requested subjects to generate correction commands, by leading the drone in counter direction to the wrong commands, in order to guide the drone back to the preset flight course.

The AR environment in both the investigation and the application studies were built using Unity 3.0 (Unity Technologies

Co.) on HoloLens (Microsoft Co.). The Fig. 4(b) shows the subject I who was wearing the HoloLens, the dry-electrode EEG cap and the four-channel inMEx system in our investigation and application studies. In order to avoid false-positive detection, a ten-second eye-opened resting state EEG was recorded without viewing any flickering object. The resting-state EEG data were used in the following EEG analysis to determine valid commands. The signal processing was performed using MATLAB v2020a in both our investigate and application studies.

C. Design of Visual Stimulation Sequence Using the PA Method

In the conventional visual stimuli on CRT/LCD screen, the screen refreshing rate should be taken into account for determining the flickering frequency. The flickering frequency should be the subharmonics of 60 Hz, which means the flickering pattern should be changed between white and black states for every predetermined number of frames. For example, one reversal flickering pattern between white and black states with the reversal duration of every two frames can produce the 15 Hz visual stimulus in using a 60 Hz refreshing rate. However, some flickering frequencies, such as 11 and 13 Hz, could not be simply generated using the aforementioned reversal flickering pattern technique with changing a fixed number of frames between white and black states. Therefore, instead of using a fixed number for reversal duration (i.e., white and black states), the number of frames for state reversal should be designed adaptively for those flickering frequencies which are not located at the subharmonic frequencies of 60 Hz refreshing rate.

Since the frequency of SSVEP should accord with the frequency of visual stimulus, the number of flash onsets, i.e., the times of changing from black states to white states, should be equivalent to the cycles of the designed flickering frequency in a certain interval of time. The accumulated phase angle in a reversal duration, either a white or black state, is equivalent to the number of frames in the reversal duration multiplied by the phase angle provided by each frame. The phase angle provided by each frame can be calculated with respect to the frequency of visual stimulus, represented as:

$$PPF = f_{stim} \times (\frac{360^\circ}{f_{RR}}), \tag{1}$$

where PPF is the phase per frame with respect to f_{stim}, f_{stim} is the stimulus frequency, and f_{RR} is refreshing rate of the HMD ($f_{\mathrm{RR}} = 60$ Hz in this study).

However, in the case that the reversal phase is not the integer multiple of PPF which is not able to represent the phase of a half cycle (180°) by an exact number of frames. Therefore, the accumulated phase can be represented as:

$$\theta_{AP} = \mathrm{PPF} \times \mathrm{k} = 180^\circ \times \mathrm{M} + \Delta, \tag{2}$$

in which θ_{AP} is the phase accumulated from the first frame to the k^{th} frame, k is the index of current frame, M is the reversal times of our flickering sequence from the initial frame, and Δ is the residual difference between the accumulated phase θ_{AP} and the accumulated phase after M time reversals. Therefore, the question to determine the brightness state of k^{th} frame is to decide whether the k^{th} frame should reverse its brightness state or not. For example, a virtual object flickers at 11 Hz with $PPF = 66^\circ$, the θ_{AP} is 264° at fourth frame ($k = 4$) with $M = 1$ and $\Delta = 84^\circ$, according to Eq. (2). In the continuing fifth frame ($k = 5$), the θ_{AP} is 330° and then we have $\Delta = 150^\circ$ for $M = 1$ and $\Delta = -30^\circ$ for $M = 2$, respectively. Therefore, choosing $M = 2$ can reduce the phase difference of our generated flickering sequence and the desired accumulated phase angle θ_{AP}. Because M represents the reversal times, the change of M indicates the brightness state at the fifth frame should be changed from the fourth frame. Accordingly, the determination of the brightness state of the k^{th} frame can be considered as the problem to minimize the phase difference between the accumulated phase θ_{AP} and the phase resulted from reversal times of our flickering sequence. In other words, we want to control the brightness state of each frame to make the phase of the generated stimulation sequence approaching the accumulated phase in ideal condition. We thereof intend to seek a number M to minimize the absolute value of phase angle Δ, represented as:

$$M^* = Arg_M \min\left\{\left|180^\circ \times M - PPF \times k\right|\right\}, \tag{3}$$

where M^* is the optimal integer for minimize Δ. Since the M^* is the number of reversal times from the beginning to the k^{th} frame, the brightness state of the k^{th} frame should be equaled (or changed) for odd (or even) number of M^*, compared to the brightness state of the first frame. For the k^{th} frame with M reversal times at the $(k-1)^{\mathrm{th}}$ frame, the determination of the brightness state for the k^{th} frame can be achieved by testing whether $M^* = M$ or $M^* = M + 1$ has smaller absolute value of residual phase difference, $|\Delta|$. Therefore, if the $|\Delta|$ calculated from (2) is smaller by giving $M^* = M + 1$, then the brightness state should be changed from the $(k-1)^{\mathrm{th}}$ frame to the k^{th} frame. The stimulation sequence generated by the aforementioned PA method in (3) is denoted as phase-approaching stimulation (PAS) sequence. The pseudo code for the generation of the PAS sequence is shown in Fig. 5.

D. Visual Target Detection Using Canonical Correlation Accuracy Method

The canonical correlation accuracy (CCA) was adopted to detect the gazed target in this study. Considering two data sets, one is the four-channel EEG signals and the other contains the sinusoidal reference signals of our six stimulation frequencies. The CCA tries to maximize the linear correlation between the two data sets by means of finding two projection vectors w_x and w_y. In this study, the gaze-target was detected every one second (500 sample points). The four-channel recorded EEG signals were arranged in a X_{CxN} matrix ($C = 4$ and $N = 1000$) and the matrix of reference $\mathrm{Y_{MxN}}$ ($M = 4 \times F$ and $N = 1000$) was set to include the first and second harmonic frequencies of each stimulation frequency f_i, $i = 1, 2 \ldots, F$, where F is the number of stimulation frequencies in the study ($F = 12$ for the investigation study and $F = 6$ for the application study).

Algorithm: PAS-sequence generation

1. $f_{stim} \leftarrow$ Choose frequency stimulus
2. $PPF = f_{stim} \times (360/f_{RR})$
3. $k \leftarrow$ Choose the kth frame
4. θ_{AP} = PPF × k
5. $M_1 \leftarrow \theta_{AP}$ mod 180
6. $\Delta_1 \leftarrow |$ PPF × k – 180 × $M_1|$
7. $M_2 \leftarrow M_1 + 1$
8. $\Delta_2 \leftarrow |$ PPF × k – 180 × $M_2|$
9. if $\Delta_2 < \Delta_1$ then
10. change the brightness state from the k-1th frame
11. else
12. maintain the brightness state from the k-1th frame
13. end if

Fig. 5. The pseudo code of the proposed PAS sequence.

The matrix of reference signal Y_i for stimulation frequency f_i was represented as:

$$Y_i = \begin{bmatrix} \sin(2\pi f_i n \Delta T) \\ \cos(2\pi f_i n \Delta T) \\ \sin(2\pi (2f_i) n \Delta T) \\ \cos(2\pi (2f_i) n \Delta T) \end{bmatrix} \quad (4)$$

where f_i was the i^{th} stimulus frequency, n was the n^{th} data sample ($n = 1, 2, 3, \ldots, N$), ΔT was the sampled duration ($\Delta T = 1/F_s$), and F_s was the sampling rate. CCA explored two vectors w_x and w_y to maximize the linear correlation C_i in (5).

$$C_i = \frac{E\left[w_x^T X Y_i^T w_y\right]}{\sqrt{E\left[w_x^T X X^T w_x\right] E\left[w_y^T Y_i Y_i^T w_y\right]}}, \quad (5)$$

The output canonical correlation C_i obtained from different stimulation frequencies were compared, and the C_{max} with maximum value of canonical correlation was identified, i.e., $C_{max} = \max\{C_i, i = (1, 2, \ldots, F)\}$. The virtual object i_{gaze} corresponding to the maximum canonical correlation C_{max} was recognized as the gazed target, and the drone movement command of the recognized gazed target was executed.

In this study, the canonical correlation values were calculated every two seconds. To prevent false-positive command output, a threshold C_{th} was determined from the resting state recordings of the twenty participants. The C_{th} was determined as the mean plus two times the standard deviation of the canonical correlation from the resting state recordings. Only those EEG segments with C_{max} higher than the C_{th} was designated as valid command and its corresponding drone movement was executed.

E. Drone Flying Setting and the Evaluation of Online Performance on the HMD-Based BCI System

We proposed the PAS sequence to design visual stimulator on HoloLens for implementing SSVEP-based BCI. In our application study, the proposed SSVEP-based BCI transmitted the detected command by WIFI to the drone. After receiving the BCI command, the drone was operated the corresponding movement with the fixed speed (1 m/s) for 1 s. The current setup in our application study was to detect the gaze-target every 1 s with 50% overlap and to confirm it as a valid output of BCI command after 3 consecutively successful detections. Each successful detection should confirm that the C_{max} is larger than the C_{th} ($C_{th} = 0.33$ in the application study).

In order to evaluate the performance of BCI, the ITR has been widely used as benchmark in many studies [22]. The ITR was calculated as:

$$\frac{Bits}{Command} = log_2 N + Acc \cdot log_2 Acc + (1 - Acc) log_2 \left(\frac{1 - Acc}{N - 1}\right), \quad (6)$$

$$ITR = \frac{Bits}{Command} \times \frac{60}{CTI}, \quad (7)$$

where N is the total number of visual targets ($N = 6$ in the application study), Acc was calculated by the summation of correct and correction commands divided by the total valid commands and the command transfer interval (CTI) was determined by the total execution time divided by the number of total valid BCI commands.

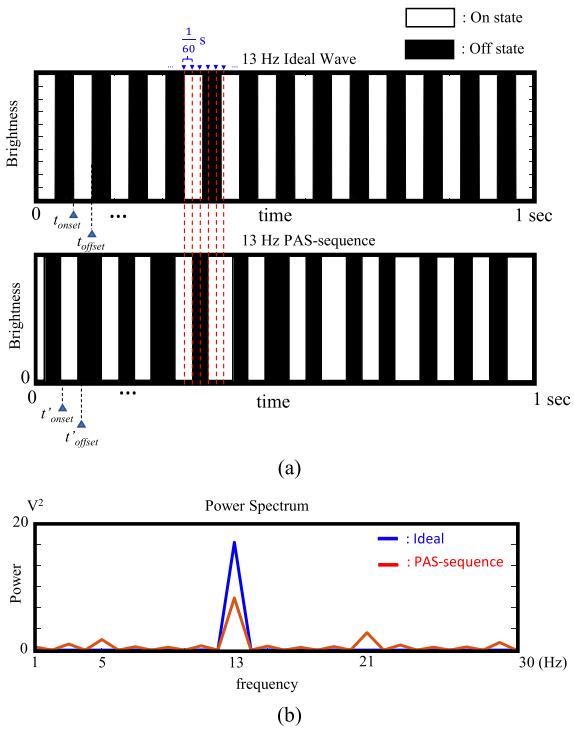

Fig. 6. (a) The upper panel is a 13 Hz ideal wave and the lower panel is a 13 Hz PAS-sequence. (b) The Fourier spectra between 13 Hz PAS-sequence (red line) and the ideal 13 Hz square wave (blue line).

III. Results

Fig. 6 demonstrates the comparison of a 13 Hz PAS sequence designed with an ideal 13 Hz square wave (simulated by 24000 Hz screen refreshing rate). The red dashed lines

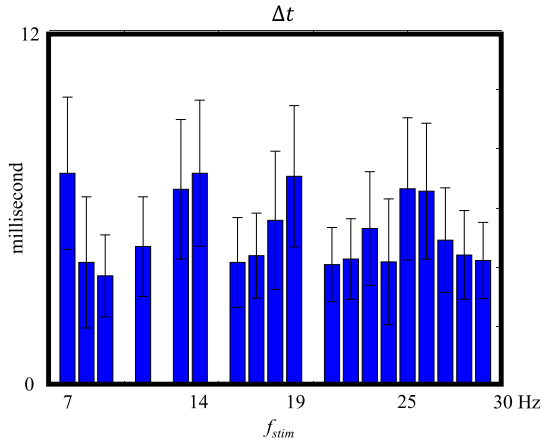

Fig. 7. The difference of the onset times between the PAS sequence and idea square waves at stimulation frequencies from 7 to 30 Hz. The box and the whisker in each bar show the mean and the standard deviation, respectively.

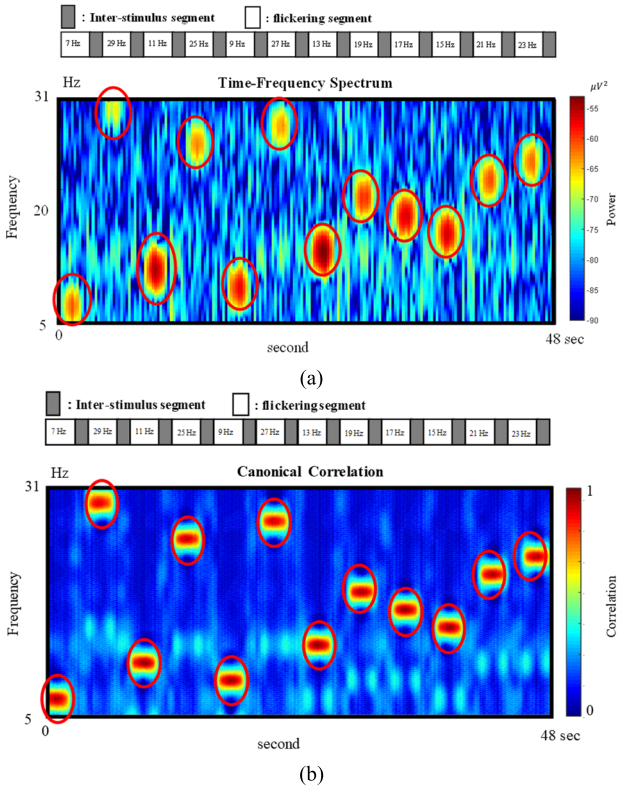

Fig. 8. The values of (a) short-time Fourier transform analysis and (b) the canonical correlation C_i of the measured SSVEPs from subject S_1.

show the start time of each frame at 60Hz refreshing rate. The stimulation sequences and Fourier spectra of the 13 Hz PAS sequence and the 13 Hz square wave are shown in Fig. 6(a) and Fig. 6(b), respectively. It can be observed in upper panel of Fig. 6(a) that most of the reversal times (dark-to-bright or bright-to-dark) are not synchronized to the start time of the frames (marked by blue inverted triangles). It indicates the flickering frequencies, which are not located at the subharmonic frequencies of the refreshing rate (60 Hz), are not able to be generated on a fixed-frame rate displayer. In contrast, the PAS sequence in the lower panel of Fig. 6(a) considered the brightness frame-by-frame to minimize the difference of the accumulated phase between PAS sequence and ideal square wave. The reversal times were designed to match the start times of frames so that the PAS sequence can be easily implemented. Fig. 6(b) shows the comparison of the Fourier spectra between the 13 Hz PAS sequence and the ideal 13 Hz square wave. It can be observed that both the two waves have clear 13 Hz peaks on the Fourier spectra. However, the power leakage in 13 Hz PAS sequence is larger than that in the ideal 13 Hz square wave, resulting from the mismatch between the two sequences. The PAS sequence adaptively adjusts the brightness state of its current frame to pursue the accumulated phase of the ideal wave, in which sacrifices the consistency in sequence repeatability and causes larger spectral leakage.

Since it has been known that the SSVEP is only related to the timing of onset time (t_{onset}) of flickering stimuli (see Fig. 6(a)), it is interesting to see the difference of onset times between PAS sequence and ideal square waves across different frequencies. The difference of the onset times (Δt) between the PAS sequence and ideal square waves at stimulation frequencies from 7 to 30 Hz were shown in Fig. 7. The frequency increment for the stimulation frequencies was 1 Hz. Stimulation frequency higher than 30Hz was beyond the Nyquist frequency of 60Hz refreshing rate and not included in this onset time examination. It can be observed in Fig. 7 that the time difference between the sequences was zero at the subharmonic frequencies (i.e., 10, 12, 15, 20, and 30 Hz) of the 60 Hz refreshing rate, since the reversal times at these frequencies were exactly occurred at the start time of frames at 60 Hz refreshing rate. For stimulation frequencies not located at those subharmonic frequencies, the mean and standard deviation indicated the level of how the PAS sequence was adjusted to maintain the intended stimulation frequencies. The time difference of onset timing between the ideal and the PAS sequences were shown in TABLE I. The Δt had larger values at the 7, 11, 14, 19, 25 Hz. All the Δt are less than the half of one frame with 60 Hz screen refreshing rate (8.3 ms).

Fig. 8(a) and 8(b) demonstrate the values of short-time Fourier transform (STFT) analysis (1 s Hamming window with 50% overlap; Oz channel) and the canonical correlation C_i of the measured SSVEPs from S_1 in our investigation study, respectively. The order of the stimulation frequencies is shown in the upper panel in both Fig. 8(a) and 8(b). In Fig. 8(a), the STFT values showed maximum power at the designated stimulation frequencies (marked by red elliptic circle) within each flickering segment which indicated the SSVEPs were successfully induced by the generated PAS sequence. In Fig. 8(b), the utilization of CCA effectively suppressed the background disturbances and achieved better discrimination for the gazed-target (marked by red elliptic circle) detections.

To demonstrate the capabilities of STFT and CCA in avoiding false-positive detections, the values of STFT (as shown in Fig. 9(a)) and canonical correlations C_i (as shown in Fig. 9(b)) in the gaze and non-gaze (resting state) conditions were compared. Both the values calculated from STFT and

TABLE I
THE TIME DIFFERENCE OF ONSET TIMING BETWEEN THE IDEAL AND THE PAS-SEQUENCES

Frequency Hz	Time Difference ms	Frequency Hz	Time Difference ms	Frequency Hz	Time Difference ms
7	7.18 ± 5.14	15	0.00 ± 0.00	23	5.31 ± 3.84
8	4.17 ± 4.43	16	4.17 ± 3.03	24	4.19 ± 4.26
9	3.72 ± 2.77	17	4.40 ± 2.87	25	6.65 ± 4.80
10	0.00 ± 0.00	18	5.59 ± 4.67	26	6.58 ± 4.60
11	4.70 ± 3.37	19	7.08 ± 4.77	27	4.92 ± 3.54
12	0.00 ± 0.00	20	0.00 ± 0.00	28	4.42 ± 3.00
13	6.64 ± 4.72	21	4.09 ± 2.51	29	4.24 ± 2.58
14	7.18 ± 4.94	22	4.28 ± 2.72	30	0.00 ± 0.00

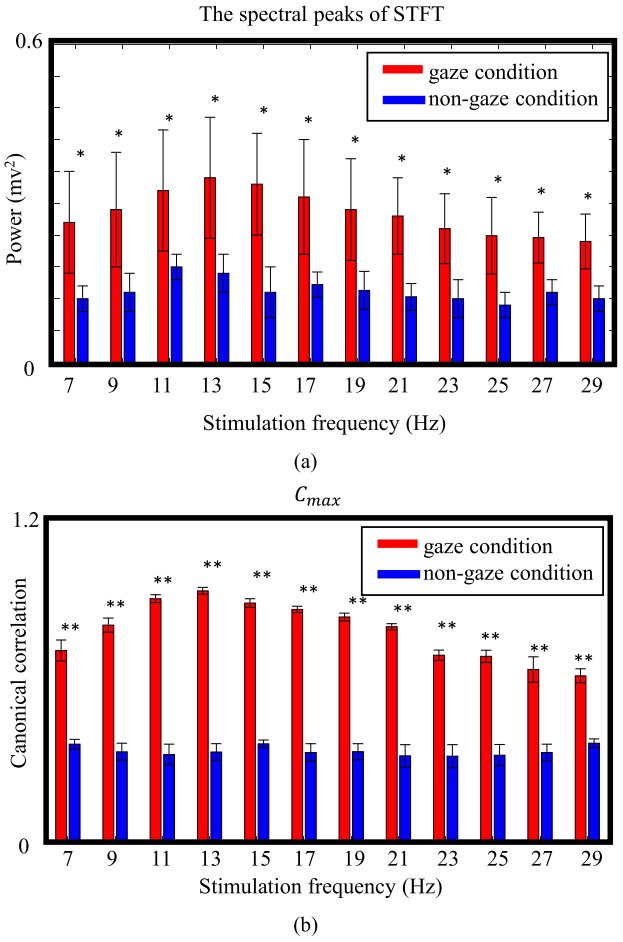

Fig. 9. The comparison of gaze and non-gaze conditions in (a) the spectral peaks of STFT and (b) the canonical correlation C_i of CCA. * and ** indicate significant difference between conditions at $\rho < 0.05$ and $\rho < 0.01$, respectively. The box and the whisker in each bar show the mean and the standard deviation, respectively.

CCA showed significant differences between the gazed and non-gazed conditions at all stimulation frequencies (matched-pair Wilcoxon test, $\rho < 0.05$ for STFT; matched-pair Wilcoxon test, $\rho < 0.01$ for CCA). TABLE II lists the spectral peaks of STFT and the canonical correlation C_i of CCA in the gaze and non-gaze conditions.

In order to choose the suitable window size for our application study, gaze-target detections in viewing a virtual object with 19, 21, 23, 25, 27, and 29 Hz frequencies with different time window sizes, from 0.5 to 1.5 s in 0.25 step, were tested, and the detection accuracies resulted from different window sizes were analyzed using CCA. The detection accuracies were 85.55 ± 10.23, 90.55 ± 9.55, 95.12 ± 7.56, 98.22 ± 6.33, and $99.12 \pm 5.23\%$ for 0.50, 0.75, 1.00, 1.25, and 1.50 s window sizes, respectively. The 1 s window size which generated the high detection accuracy (>95%) was then chosen as the window size for drone control in our application study. Table III demonstrates the valid commands ($C_{max} > 0.33$) generated from the twenty subjects in our application study. The subject index, sequence of valid commands, Acc, execution time, CTI, and ITR of the twenty participants are listed in the first to sixth columns, respectively. In the second column, the correct commands, the wrong commands (marked with underlines), and the correction commands (marked by circles) are listed. Since the flying time of the drone was programmed as one second per command, the flying time in Table III didn't include the execution time so that the CTI and ITR can reflect the pure BCI performance. The Acc, execution time, CTI, and ITR over the twenty subjects (mean $\pm$ std.) were 93.30 ± 2.52 %, 47.25 ± 2.90 s, 3.40 ± 0.15 s/command and 36.84 ± 3.04 bits/min, respectively.

IV. DISCUSSION

In this study, we have demonstrated the feasibility of the PA method to synthesize user-specified stimulation frequency on the HMD with a fixed frame rate. The SSVEP can be induced by the arbitrary frequency, which is lower than the half of the frame rate. In contrast to other SSVEP-based BCI studies using visual stimulator with fixed-frame rate, the choices of stimulation frequencies were limited to the sub-harmonic frequencies of the screen refreshing frequency. For example, only six stimulation frequencies (6 Hz, 10 Hz, 12 Hz, 15 Hz, 20 Hz, and 30 Hz) can be chosen for BCI control with a 60 Hz HMD. The proposed PA method generates PAS sequence to synthesize arbitrary user-specified stimulation frequencies, in which the stimulation frequencies were lower than half of the refreshing frequency owing to the Nyquist theorem. The PA method recursively checks the accumulated phase

TABLE II
THE SPECTRAL PEAKS OF STFT AND CANONICAL CORRELATION

Frequency Hz	Spectral Peaks of STFT		Canonical Correlation C_i of CCA	
	Gaze Condition μV^2	Non-Gaze Condition μV^2	Gaze Condition	Non-Gaze Condition
7	0.22 ± 0.08	0.10 ± 0.02	0.71 ± 0.04	0.36 ± 0.02
9	0.24 ± 0.09	0.11 ± 0.03	0.81 ± 0.03	0.33 ± 0.03
11	0.27 ± 0.10	0.15 ± 0.02	0.91 ± 0.01	0.32 ± 0.04
13	0.29 ± 0.10	0.14 ± 0.03	0.94 ± 0.01	0.33 ± 0.03
15	0.28 ± 0.08	0.11 ± 0.04	0.89 ± 0.02	0.36 ± 0.01
17	0.26 ± 0.09	0.12 ± 0.02	0.87 ± 0.01	0.33 ± 0.03
19	0.24 ± 0.08	0.11 ± 0.03	0.84 ± 0.01	0.33 ± 0.03
21	0.23 ± 0.06	0.10 ± 0.02	0.80 ± 0.01	0.31 ± 0.04
23	0.21 ± 0.06	0.10 ± 0.03	0.69 ± 0.02	0.32 ± 0.04
25	0.20 ± 0.06	0.09 ± 0.02	0.68 ± 0.02	0.32 ± 0.04
27	0.19 ± 0.04	0.11 ± 0.02	0.64 ± 0.05	0.33 ± 0.03
29	0.19 ± 0.04	0.10 ± 0.02	0.62 ± 0.03	0.36 ± 0.02

TABLE III
THE PERFORMANCE OF BCI DRONE CONTROL

Subject index	Command Sequence	Acc (%)	Execution time (s)	CTI (s/command)	ITR (bits/min)
S1	↑→↓ F ← B ↑→↓ F ← B	12/12 (100.00%)	42.00	3.50	44.31
S2	↑→↓F ←→⊖B ↑→↓ F ← B	13/14 (92.86 %)	49.00	3.50	35.11
S3	↑→↓ F ← B ↑ ↑⓪→↓ F ← B	13/14 (92.86 %)	48.00	3.43	35.84
S4	↑→↓ F ↑⓪← B ↑→↓ F ← B	13/14 (92.86 %)	49.00	3.50	35.11
S5	↑→↓ F ← B ↑→↓ F ← B	12/12 (100.00%)	42.00	3.50	44.31
S6	↑→↓ F ← B ↑ ↑⓪→↓ F ←←⊖B	14/16 (87.50 %)	53.00	3.31	31.72
S7	↑→↓ F ↑⓪← B ↑→↓ F ← B	13/14 (92.86 %)	54.00	3.86	31.86
S8	↑→↓ F ↑⓪← B ↑→↓ F ← B	13/14 (92.86 %)	47.00	3.36	36.60
S9	↑→←⊖↓ F ← B ↑→↓ F ← B	13/14 (92.86 %)	48.00	3.43	35.84
S10	↑→↓ F ← B ↑ ↓⓪→↓ F ← B	13/14 (92.86 %)	50.00	3.57	34.40
S11	↑→↓ F ← B ←⊖↑→↓ F ← B	13/14 (92.86 %)	47.00	3.36	36.60
S12	↑→↓ F ← B ↑ →↓←⊖F ← B	13/14 (92.86 %)	48.00	3.43	35.84
S13	↑→↓ F ← B ↑ →↓←⊖F ← B	13/14 (92.86 %)	45.00	3.21	38.23
S14	↑→↓ F ← B ↑ ↑⓪→↓ F ← B	13/14 (92.86 %)	47.00	3.36	36.60
S15	↑←⊖→↓ F ← B ↑→↓ F ← B	13/14 (92.86 %)	46.00	3.29	37.40
S16	↑→↓ F ←→⊖B ↑→↓ F ← B	13/14 (92.86 %)	47.00	3.36	36.60
S17	↑→↓ F ← B ←⊖↑→↓ F ← B	13/14 (92.86 %)	45.00	3.21	38.23
S18	↑→↓ ↓⓪F ← B ↑→↓ F ← B	13/14 (92.86 %)	45.00	3.21	38.23
S19	↑→↓ F ←→⊖ B ↑→↓ F ← B	13/14 (92.86 %)	46.00	3.29	37.40
S20	↑→↓ F ← B ↑ ↑⓪→↓ F ← B	13/14 (92.86 %)	47.00	3.36	36.60
Averaging		93.30 ± 2.52 %	47.25 ± 2.90	3.40 ± 0.15	36.84 ± 3.04

of the stimulation sequence and uses it as an indicator to determine the illuminance state of next frame, in order to match the accumulated phases between the ideal condition and the generated PAS sequence. In our study, six PAS sequences were generated in high frequency range (19∼29 Hz) to induce subject's SSVEPs for real-time drone control. The feasibility of PA method to implement an SSVEP-based on a fixed-frame HMD is therefore demonstrated.

The SSVEP induced by the PAS sequence has been validated in our investigation study. In Fig. 9, it can be observed that the frequency of SSVEP was the same as the flickering frequency of the virtual object. The SSVEPs induced by the flickering virtual object, driven by PAS sequences of different frequencies, also showed an amplitude-frequency preference [6]. The amplitudes of SSVEPs in the gaze condition were significantly larger than those in the non-gaze condition (resting state) at all stimulation frequencies. It means that the PAS sequence effectively induced the SSVEPs at our desired stimulation frequencies, so that we can use the PAS sequence to implement an SSVEP-based BCI with commands more than the subharmonic number of the refreshing rate on an HMD.

The present PA method controls the brightness state of each frame to minimize the difference of accumulated phases between our PAS sequence and the ideal wave. For those stimulation frequencies not at the subharmonic frequencies of screen refreshing rate, the PAS sequences are not simply the concatenation of repetitive ON-OFF states which can become broadened in the spectra compared to ideal waves.

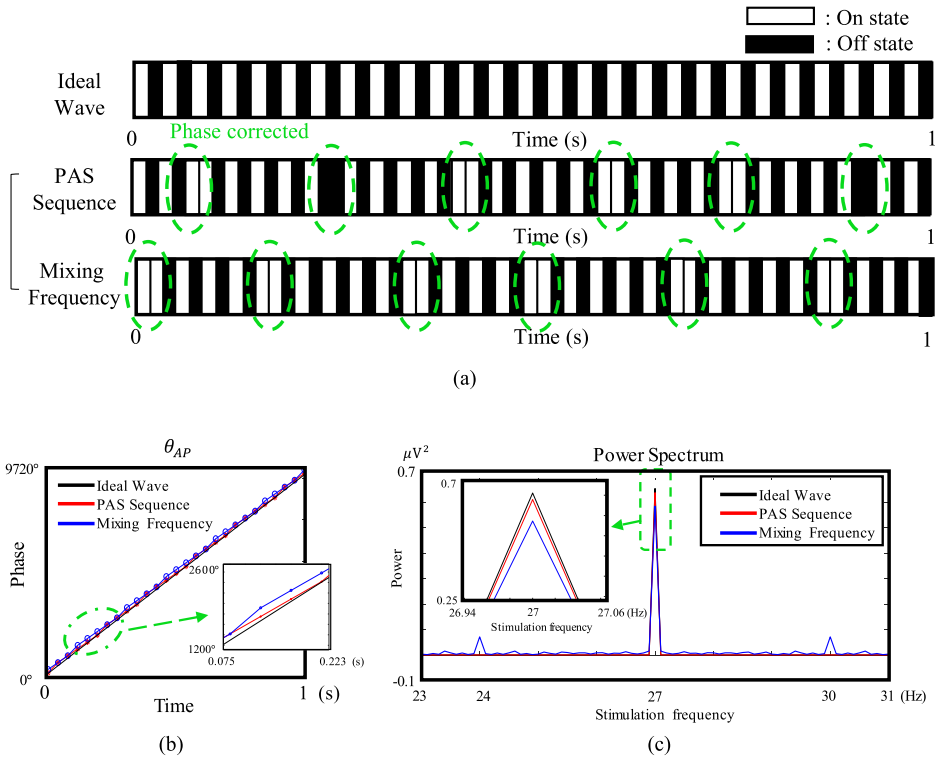

Fig. 10. (a) the 27 Hz ON/OFF states of the ideal wave (the first panel), the PAS sequence (the second panel), and the mixing-frequency method (the third panel), and these three sequences' respective (b) the accumulated phases, θ_{AP}, and (c) the Fourier spectra.

To illustrate the phase approaching mechanism of our PA method, the stimulation sequence, accumulated phase and the Fourier spectra of our PAS sequence at 27 Hz stimulation frequency were illustrated in Fig. 10. For the comparison purpose, the stimulation sequence, accumulated phase and the Fourier spectrum generated from mixing-frequency approximation method [18] were also plotted. Fig. 10(a) shows the 27 Hz ON/OFF states of the ideal wave, the PAS sequence, and the mixing-frequency method. The upper panel in Fig. 10(a) shows the ON-OFF state of a 27 Hz ideal wave, in which the timing was precisely controlled irrelevant to the timing of screen refreshing rate. The second and the third panels in the Fig. 10(a) are the flicking sequences generated by our PA method and the mixing-frequency method, in which the timing of the two sequences were synchronized to frame onsets of a 60 Hz display device. It can be observed that the phase corrections (marked by dashed green ellipses) were occurred in both the sequences generated by our PA method the mixing-frequency method. In Fig. 10(b), the accumulated phases, θ_{AP}, of these three sequences in one second are shown. The inserted figure presents the enlarged plot of the accumulated phase from 0.075 to 0.223 s. Compared to the accumulated phase of the sequence of mixing-frequency method, the θ_{AP} of the PAS sequence had smaller phase bias deviated from the accumulated phase of ideal wave. Calculating the mean phase differences of the two approximation methods with the ideal wave, the phase differences were $80.59° \pm 46.84°$ and $98.24° \pm 66.66°$ for the sequences generated by our PA method and the mixing-frequency method, respectively. The PAS sequence had smaller phase difference, since it aims to minimize the phase difference by adaptively adjusting the brightness state of each frame. In contrast to the mixing-frequency method, it tried to mixing the flickering blocks from two neighboring subharmonic frequencies which was not performed in a frame-by-frame consideration.

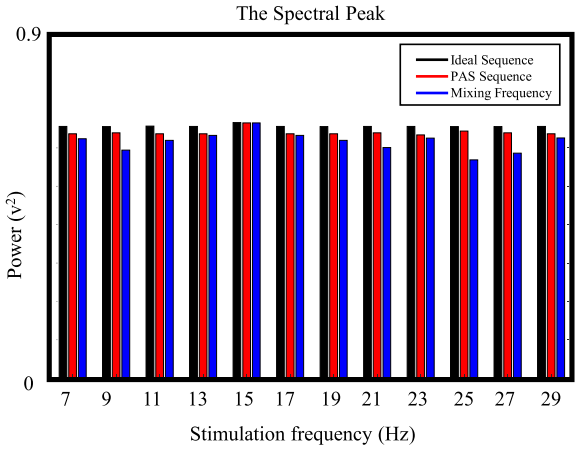

Fig. 11. The spectral peaks of the ideal wave, the PAS sequence, and the sequence of mixing-frequency method were compared from 7 to 29 Hz in 2Hz steps.

Fig. 10(c) illustrates the Fourier spectra of the three sequences shown Fig. 10(a). Among the three spectra, the spectrum of the sequence generated from the mixing-frequency method has two apparent sidelobes located at 24 and 30 Hz which resulted in a lower 27 Hz spectral peak, compared to

the spectra obtained from the ideal wave and the sequence of PA method (see the inserted figure). It echoes the observation of phase difference shown in Fig. 10(b), in which the PAS sequence tried to minimize phase difference and thereof had smaller power leakage outside the main spectral peak. In Fig. 11, the spectral peaks of the ideal wave, PAS sequence and the sequence of mixing-frequency method were compared, from 7 to 29 Hz in 2Hz steps. It can be observed that the spectral peaks of PAS sequences were all higher than the sequences of mixing-frequency method. Except for the spectral peaks at 15Hz, the 15Hz was the subharmonic frequency of the 60Hz display device. The three sequences were the same at 15 Hz and had same spectral peaks. It is worthy to notice the spectral peaks at 25 and 27Hz. The spectral peaks of mixing-frequency method had larger differences compared to the ideal waves. Because the 25 and 27Hz are away from the 20 and 30Hz sub-harmonic frequencies when using a 60Hz display device, the fast changing between the two subharmonic states might cause larger spectral leakages from the main peaks.

In our application study, the six virtual objects driven by PAS sequences with different frequencies were successfully used to control a flying drone. The gaze-target was detected every one second and a valid output required the same gaze-target to be confirmed three consecutive times [5]. Since the window size for gaze-target detection should be decided by considering a balance between the command execution speed and detection accuracy. For example, a longer window size will result in higher detection accuracy but slower execution speed. Since the 1 s window size has achieved acceptable detection accuracy ($>$95%), the window size was therefore chosen in our application study to make a compromise between the execution time and system reliability.

It has been reported that CCA has the better detection performance than the Fourier-based method [23]. It can be observed in Fig. 9 that the SSVEP can be successfully induced by the visual stimulator driven by PAS sequences across different stimulation frequencies. Although the spectral amplitude of STFT and the canonical correlation C_i of CCA were both significant in gaze condition ($<$0.05 for STFT and $<$0.01 for CCA), compared to those values in non-gaze condition, the CCA had shown its great performance in noise removal which had achieved more prominent statistical significance as shown in Fig. 9. The signal processing power of CCA has been mentioned in several studies, especially in SSVEP-based BCI applications [24]. Bin *et al.* claimed that CCA has ability to improve the SNR of SSVEP which results in increasing detection accuracy of BCI usage [25]. With CCA, in our application study, the detection accuracies and ITR had achieved higher than 90% and 35 bits/min, respectively, in all subjects (see Table III). Taking the data from the application study and reprocessing them with STFT, we found the detection accuracy and ITR became 87.35% and 28.15 bits/min, respectively, which were lower than the results from CCA processing.

In this study, we designed a visual stimulator driven by the PAS sequence on HMD. Compared to the traditional visual stimulator, such as CRT/LCD screen, the HMD has advantages of the portability design and easy to arrange multiple stimuli in VR/AR. Moreover, the illuminance state of each stimulus can be determined independently in frame-by-frame. Considering flickering fusion effect using higher stimulation frequency, we chose six frequencies higher than 19 Hz for better visualization in our application study. However, compared to previous BCI studies on VR device, the available target number were few ($<$6 commands) owing to the limitation of available number of subharmonic frequencies with fixed frame rate. Wang *et al.* designed BCI commands at four subharmonic frequencies (6.4, 7.5, 9.0, and 11.25 Hz on a 90Hz HMD) to control a flying drone [15]. Stawicki *et al.* implemented a three-command SSVEP-based BCI using three subharmonic frequencies (7.2, 9.0 and 12.0 Hz) on a 72 Hz HMD to control a robot car [14]. In the aforementioned studies, the available command number and the stimulation frequencies were low which led to lower ITRs and poor visualization. With the use of PA method for virtual object flickering, the number of available stimulation frequencies is no longer limited to the subharmonic frequency number on HoloLens, which expands the usability of HMD in SSVEP-based BCI studies.

V. Conclusion

In this study, we have demonstrated the feasibility of the PA method to synthesize user-specified stimulation frequency on the HMD with a fixed frame rate. In order to increase the available number of targets on a displayer with a fixed frame rate, the proposed PA method can generate arbitrary user's designed stimulation frequencies for BCI control. The PAS sequence effectively induced the SSVEPs at our desired stimulation frequencies, so that we can use the PAS sequence to implement an SSVEP-based BCI. The six-command wearable frequency-coded SSVEP BCI has been implemented successfully, which controlled a flying drone successfully with the 93.30 $\pm$ 2.52% of accuracy and 36.84 $\pm$ 3.04 bits/min of ITR.

References

[1] N. Birbaumer *et al.*, "A spelling device for the paralysed," *Nature*, vol. 398, no. 6725, pp. 297–298, 1999.

[2] J. A. Pineda, B. Allison, and A. Vankov, "The effects of self-movement, observation, and imagination on μ rhythms and readiness potentials (RP's): Toward a brain-computer interface (BCI)," *IEEE Trans. Rehabil. Eng.*, vol. 8, no. 2, pp. 219–222, Jun. 2000.

[3] E. Donchin, K. M. Spencer, and R. Wijesinghe, "The mental prosthesis: Assessing the speed of a P300-based brain-computer interface," *IEEE Trans. Rehabil. Eng.*, vol. 8, no. 2, pp. 174–179, Jun. 2000.

[4] D. Huang, K. Qian, D.-Y. Fei, W. Jia, X. Chen, and O. Bai, "Electroencephalography (EEG)-based brain-computer interface (BCI): A 2-D virtual wheelchair control based on event-related desynchronization/synchronization and state control," *IEEE Trans. Neural Syst. Rehabil. Eng.*, vol. 20, no. 3, pp. 379–388, May 2012.

[5] P.-L. Lee, J.-C. Hsieh, C.-H. Wu, K.-K. Shyu, and Y.-T. Wu, "Brain computer interface using flash onset and offset visual evoked potentials," *Clin. Neurophysiol.*, vol. 119, no. 3, pp. 605–616, Mar. 2008.

[6] H.-T. Hsu *et al.*, "Evaluate the feasibility of using frontal SSVEP to implement an SSVEP-based BCI in young, elderly and ALS groups," *IEEE Trans. Neural Syst. Rehabil. Eng.*, vol. 24, no. 5, pp. 603–615, May 2016.

[7] Y. Wang and T.-P. Jung, "Visual stimulus design for high-rate SSVEP BCI," *Electron. Lett.*, vol. 46, no. 15, pp. 1057–1058, 2010.

[8] R. Ortner, B. Z. Allison, G. Korisek, H. Gaggl, and G. Pfurtscheller, "An SSVEP BCI to control a hand orthosis for persons with tetraplegia," *IEEE Trans. Neural Syst. Rehabil. Eng.*, vol. 19, no. 1, pp. 1–5, Feb. 2011.

[9] H.-T. Hsu, P.-L. Lee, and K.-K. Shyu, "Improvement of classification accuracy in a phase-tagged steady-state visual evoked potential-based brain-computer interface using adaptive neuron-fuzzy classifier," *Int. J. Fuzzy Syst.*, vol. 19, no. 2, pp. 542–552, Apr. 2017.

[10] B. Koo, H.-G. Lee, Y. Nam, and S. Choi, "Immersive BCI with SSVEP in VR head-mounted display," in *Proc. 37th Annu. Int. Conf. IEEE Eng. Med. Biol. Soc. (EMBC)*, Aug. 2015, pp. 1103–1106.

[11] M. Wang, R. Li, R. Zhang, G. Li, and D. Zhang, "A wearable SSVEP-based BCI system for quadcopter control using head-mounted device," *IEEE Access*, vol. 6, pp. 26789–26798, 2018.

[12] H. Si-Mohammed *et al.*, "Towards BCI-based interfaces for augmented reality: Feasibility, design and evaluation," *IEEE Trans. Vis. Comput. Graphics*, vol. 26, no. 3, pp. 1608–1621, Mar. 2020.

[13] I. Volosyak, H. Cecotti, and A. Graser, "Optimal visual stimuli on LCD screens for SSVEP based brain-computer interfaces," in *Proc. 4th Int. IEEE/EMBS Conf. Neural Eng.*, Apr. 2009, pp. 447–450.

[14] P. Stawicki, F. Gembler, R. Grichnik, and I. Volosyak, "Remote steering of a mobile robotic car by means of VR-based SSVEP BCI," in *Proc. Int. Work-Conf. Artif. Neural Netw.* Cham, Switzerland: Springer, 2019, pp. 406–417.

[15] M. Wang, R. Li, R. Zhang, G. Li, and D. Zhang, "A wearable SSVEP-based BCI system for quadcopter control using head-mounted device," *IEEE Access*, vol. 6, pp. 26789–26798, 2018.

[16] P. Stawicki *et al.*, "Investigating spatial awareness within an SSVEP-based BCI in virtual reality," in *Proc. IEEE Int. Conf. Syst., Man, Cybern. (SMC)*, Oct. 2018, pp. 615–618.

[17] X. Chen, Z. Chen, S. Gao, and X. Gao, "A high-ITR SSVEP-based BCI speller," *Brain-Comput. Interfaces*, vol. 1, nos. 3–4, pp. 181–191, 2014.

[18] M. Nakanishi, Y. Wang, Y.-T. Wang, Y. Mitsukura, and T.-P. Jung, "Generating visual flickers for eliciting robust steady-state visual evoked potentials at flexible frequencies using monitor refresh rate," *PLoS ONE*, vol. 9, no. 6, Jun. 2014, Art. no. e99235.

[19] R. W. Homan, J. Herman, and P. Purdy, "Cerebral location of international 10–20 system electrode placement," *Electroencephalogr. Clin. Neurophysiol.*, vol. 66, no. 4, pp. 376–382, Apr. 1987.

[20] Y. Wang, R. Wang, X. Gao, B. Hong, and S. Gao, "A practical VEP-based brain-computer interface," *IEEE Trans. Neural Syst. Rehabil. Eng.*, vol. 14, no. 2, pp. 234–240, Jun. 2006.

[21] W. Yijun, W. Ruiping, G. Xiaorong, and G. Shangkai, "Brain-computer interface based on the high-frequency steady-state visual evoked potential," in *Proc. 1st Int. Conf. Neural Interface Control*, 2005, pp. 37–39.

[22] D. J. McFarland, W. A. Sarnacki, and J. R. Wolpaw, "Brain-computer interface (BCI) operation: Optimizing information transfer rates," *Biol. Psychol.*, vol. 63, no. 3, pp. 237–251, 2003.

[23] G. Hakvoort, B. Reuderink, and M. Obbink, "Comparison of PSDA and CCA detection methods in a SSVEP-based BCI-system," Centre Telematics Inf. Technol., Univ. Twente, Enschede, The Netherlands, Tech. Rep. TR-CTIT-11-03, 2011.

[24] Z. Lin, C. Zhang, W. Wu, and X. Gao, "Frequency recognition based on canonical correlation analysis for SSVEP-based BCIs," *IEEE Trans. Biomed. Eng.*, vol. 53, no. 12, pp. 2610–2614, Dec. 2006.

[25] G. Bin, X. Gao, Z. Yan, B. Hong, and S. Gao, "An online multi-channel SSVEP-based brain-computer interface using a canonical correlation analysis method," *J. Neural Eng.*, vol. 6, no. 4, Aug. 2009, Art. no. 046002.